Enhanced Shubnikov–De Haas Oscillation in Nitrogen-Doped Graphene

Han-Chun Wu,[*,†] Mourad Abid,[‡] Ye-Cun Wu,[†] Cormac Ó Coileáin,[†,§] Askar Syrlybekov,[§] Jun Feng Han,[†] Cheng Lin Heng,[†] Huajun Liu,[⊥] Mohamed Abid,[‡] and Igor Shvets[§]

[†]School of Physics, Beijing Institute of Technology, Beijing 100081, People's Republic of China, [‡]KSU-Aramco Center, King Saud University, Riyadh 11451, Saudi Arabia, [§]CRANN, School of Physics, Trinity College, University of Dublin, Dublin 2, Ireland, and [⊥]Institute of Plasma Physics, Chinese Academy of Sciences, Hefei 230031, People's Republic of China

ABSTRACT N-doped graphene displays many interesting properties compared with pristine graphene, which makes it a potential candidate in many applications. Here, we report that the Shubnikov–de Haas (SdH) oscillation effect in graphene can be enhanced by N-doping. We show that the amplitude of the SdH oscillation increases with N-doping and reaches around 5k Ω under a field of 14 T at 10 K for highly N-doped graphene, which is over 1 order of magnitude larger than the value found for pristine graphene devices with the same geometry. Moreover, in contrast to the well-established standard Lifshitz–Kosevich theory, the amplitude of the SdH oscillation decreases linearly with increasing temperature and persists up to a temperature of 150 K. Our results also show that the magnetoresistance (MR) in N-doped graphene increases with increasing temperature. Our results may be useful for the application of N-doped graphene in magnetic devices.

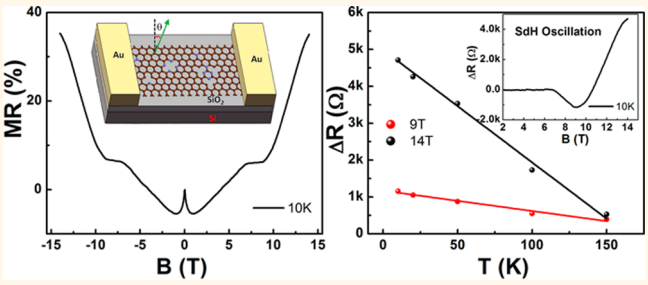

KEYWORDS: N-doped graphene · Shubnikov–de Haas oscillation · magnetoresistance · two-dimensional transport · substitutional doping

Graphene is a honeycomb-structured carbon sheet with extraordinary properties[1,2] such as a high surface area,[3] high thermal conductivity,[4] extremely high mobility,[5] and a strong Young's modulus.[6] Recently, researchers have invested considerable effort in developing reliable methods to control and tune the properties of graphene, such as patterning it into graphene nanoribbons[7,8] or graphene quantum dots.[9,10] Chemical doping, in particular substitutional doping, is an effective and important way of tailoring the electronic, chemical, optical, and magnetic properties of graphene, which has been successfully applied in carbon nanotubes and other materials.[11−15] Substitutional doping of graphene, which introduces heteroatoms, such as B, N, S, and Si, into the carbon lattice, can significantly modify its electronic properties.[16−20] Among them, N-doped graphene displays many interesting properties compared with pristine graphene, which makes it a potential candidate in many applications,[21−37] for example, enhanced catalysis for energy conversion and storage,[21−23] enhanced Li ion intercalation for lithium ion batteries,[24−26] better electron-transfer efficiency for electrochemical sensing,[27] enhanced biocompatibility for biosensing,[28−30] and an enhanced weak localization effect.[31] Moreover, N-doped graphene is also important for high-frequency semiconductor devices as a band gap can be opened using high N-doping.[17] As most applications listed above are based on the transport properties and the N-doped graphene is only a single atomic plane thick, it is very important to investigate how N-doping will affect the 2D transport properties.

In this paper, we report on the 2D transport properties of N-doped graphene, with particular attention paid to the effect of N-doping on the Shubnikov–de Haas (SdH) oscillation. The structural and chemical properties of the N-doped graphene were characterized by atomic force microscopy (AFM),

* Address correspondence to wuhc@bit.edu.cn.

Received for review April 3, 2015 and accepted June 10, 2015.

Published online June 10, 2015
10.1021/acsnano.5b02020

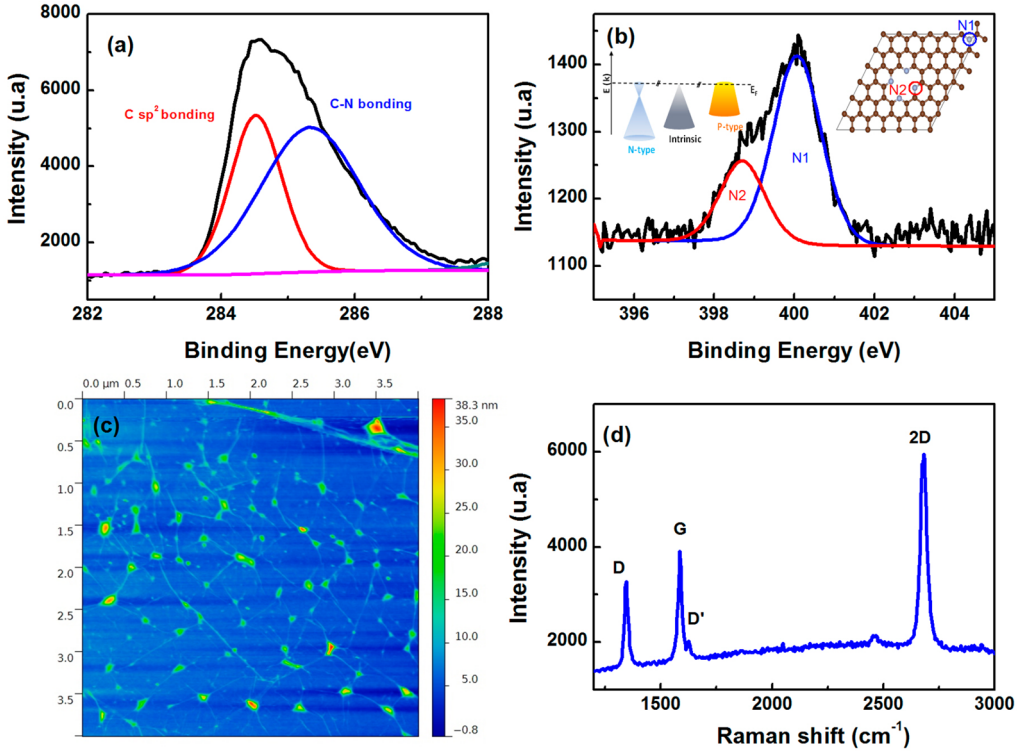

Figure 1. Characterization of nitrogen-doped graphene. X-ray photoemission spectroscopy compositional analysis for the C (a) and N (b) peaks of the nitrogen-doped graphene indicating the presence of nitrogen doping and C vacancies. (c) Typical AFM image of N-doped graphene after transfer onto SiO_2/Si substrates. (d) Typical Raman spectrum of N-doped graphene on SiO_2/Si with a 514 nm laser excitation.

X-ray photoemission spectroscopy (XPS), and Raman spectra, respectively. We observed an enhanced SdH oscillation effect in N-doped graphene, which results in stepped magneto-resistance (MR). The SdH oscillation in our N-doped graphene displays three striking features. First, the amplitude of the SdH oscillation increases with increasing N-doping and reaches more than 5k Ω at a field of 14 T. Second, in contrast to the well-established standard Lifshitz–Kosevich theory, the amplitude of the SdH oscillation decreases linearly with increasing temperature. Third, the SdH oscillation persists at temperatures up to 150 K. Our experimental results also suggest that the MR in N-doped graphene increases with increasing temperature.

RESULTS AND DISCUSSION

Device Preparation and Characterization. The single layer N-doped graphene used in this work was commercially grown, on Cu foil, purchased from Graphene Supermarket. Figure 1 shows the X-ray photoemission spectroscopy compositional analysis for the C and N peaks. The C 1s peak splits into two peaks located at 284.6 and 285.4 eV. The peak at 284.6 eV corresponds to the graphite-like sp^2 C bonding, and the peak at 285.4 eV can be attributed to C–N bonding. The large peak area of C–N bonding peak indicates that a large proportion of C atoms have been substituted by N atoms. The X-ray photoemission spectroscopy compositional analysis of the N 1s peak in Figure 1b further suggests that there are at least two distinct nitrogen configurations, *i.e.*, substitutional N located at 400.6 eV (N1) and a weak pyridine-like N signal located at 398.6 eV (N2).[38] The N-doping rate estimated from XPS characterizations is around 8%. To study the transport properties, the graphene layer was transferred onto a Si substrate with a 300 nm thick SiO_2 layer with the assistance of nitrocellulose polymer.[39] Details of the transfer process can be found in the Methods. Figure 1c shows a typical AFM image of the N-doped graphene after transfer onto the SiO_2/Si substrate. Ripples and bubbles can be observed with no nitrocellulose residues. The Raman spectrum of N-doped graphene was measured using a Renishaw inVia Raman microscope with an excitation wavelength of 514 nm (Figure 1d and Figure S1, Supporting Information). To compare, the Raman spectrum for the pristine graphene is also shown in Figure S1. The Raman spectrum of N-doped graphene shows the typical G and 2D bands at ~1586 and 2679 cm^{-1} with additional bands at ~1345 (D band), 1625 (D′ band), 2461 (D + D″), 2946 (D + D′), and 3248 cm^{-1} (2D′). The D and D′ bands are due to intervalley and intravalley double-resonance-scattering processes initiated by the presence of defects, *i.e.*, the insertion of a nitrogen dopant into the single layer graphene.[40−43] Furthermore, the nitrogen doping of single-layer graphene is accompanied by a blueshift of

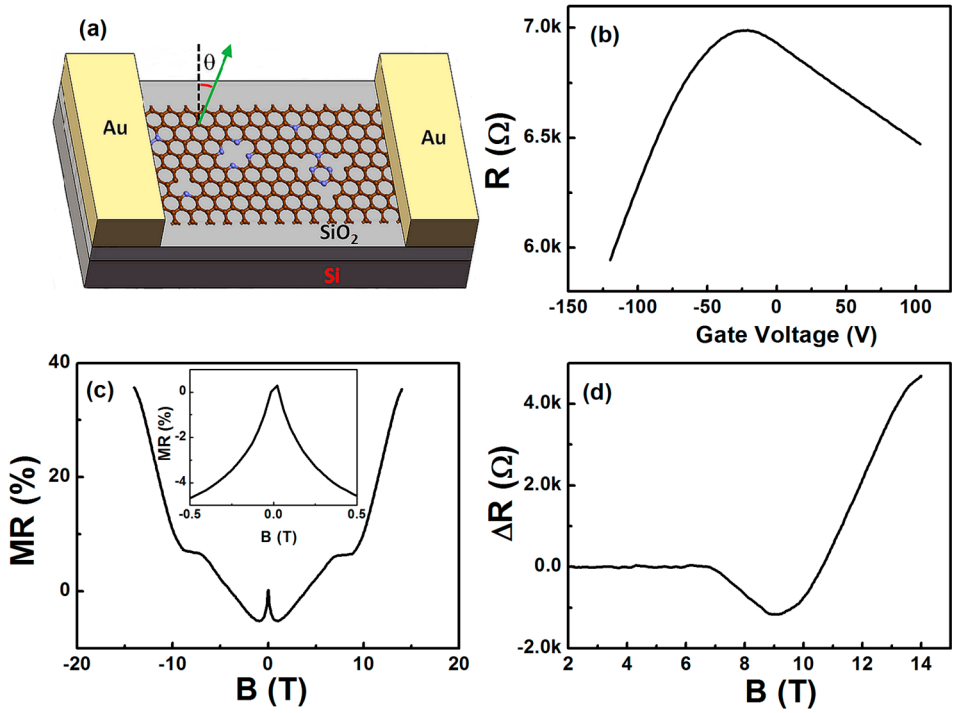

Figure 2. MR of N-doped graphene at 10 K under a perpendicular field. (a) Schematic drawing of the device. (b) Resistance as a function of the back-gate voltage with a bias voltage of 1 mV. (c) MR measured at 10 K with field perpendicular to the graphene plane. Inset: MR at low fields. (d) After subtraction of the linear MR contributions, the resistance oscillations at 10 K were measured with the field perpendicular to the graphene plane.

the G and 2D bands, which is induced by compressive strain and electron doping.

Transport Properties at 10 K under a Perpendicular Field. The transport properties of the N-doped graphene devices were measured using the two-probe method in a physical property measurement system (PPMS, Quantum Design). A schematic diagram of a typical two-terminal graphene device is shown in Figure 2a. Figure S2 shows $I-V$ curves of the two-terminal graphene devices measured at different temperatures indicating good Ohmic contact between the graphene and the electrodes. The resistance as a function of the back-gate voltage at room temperature is shown in Figure 2b. Although the resistance does not change significantly with back-gate voltage, our highly N-doped graphene does retain the property of Dirac Fermions. The Dirac point is located in the negative gate voltage region, indicating that the graphene is overall n-type due to the nitrogen doping, which is consistent with the XPS characterization as most of the nitrogen is in a N1 configuration. The field-effect mobility determined from the curve is ~1000 $cm^2/V \cdot s$ with zero gate voltage and zero magnetic field at room temperature.[44] Figure 2c shows a MR curve measured at 10 K for a field perpendicular to the graphene plane, where the MR is defined as MR = $R(B)/R(0) - 1$. Note that all of the following reported magneto-transport properties were measured with zero back-gate voltage. Interestingly, the MR curve displays stepped-like behavior, and an unsaturated positive MR of 35% is achieved at 14 T. Similar stepped MR curves were observed for other two-terminal nondoped graphene devices with graphene–metal interfaces.[45]

A more detailed analysis of the MR shows there are five distinct field regions: below 0.5 T (I), from 0.5 to 1 T (II), from 1 to 6.7 T (III), from 6.7 to 9 T (IV), and above 9 T (V). The shape of MR curve varies from one region to another. In region I, a negative MR is observed due to the weak localization effect (WL) (Figure 2c, inset). In pristine graphene, the WL effect is usually suppressed, which is attributed to the presence of the mesoscopic corrugation, such as ripples.[46] However, in our N-doped graphene, we observed an enhanced WL effect although ripples are produced during the transfer process. The enhanced WL effect in our highly N-doped graphene is due to the increased elastic intervalley scattering resulting from defects.[31] In region II, $\mu B \ll 1$, the MR curve shows a quadratic behavior and obeys the Kohler's rule. In regions III and V, the MR shows a linear response with respect to the magnetic field and the slope of the MR in region V is greater than that in region III. The linear MR in region III is usually explained using quantum linear MR[47] or by a nonuniform spatial distribution of carrier mobility.[48] Remarkably, in region IV, the resistance of the N-doped graphene remains constant. For graphene, quantum effects appear and result in resistance oscillations with the magnetic field (SdH oscillations) at magnetic fields which are strong enough for charge carriers to complete individual cyclotron orbits without

scattering, *i.e.*, $\mu B > 1$. In our N-doped graphene, the critical magnetic field is around 6.7 T. The SdH oscillation, after subtraction of the contribution due to linear MR, is plotted in Figure 2d. Interestingly, the amplitude of the SdH oscillation increases significantly with field and reaches 4700 Ω at 14 T, which is 1 order of magnitude larger than the value (300 Ω) for pristine graphene devices with the same geometry. The significantly increased amplitude of the SdH increases the slope of $\Delta R(B)$ due to the SdH oscillation. For example, in region IV, the negative slope of $\Delta R(B)$ due to the SdH oscillation is almost the same as that for the positive $\Delta R(B)$ due to the linear MR, which can explain the stepped behavior of the overall $R(B)$ in region IV. In region V, the SdH oscillation produces a positive ΔR, which is responsible for the increased slope of the MR in region V compared with region III.

Effect of N-Doping on the 2D Transport Properties. To further investigate the effect of N-doping on the SdH oscillations, we compared the SdH oscillations for devices with two different doping rates measured at 2 K under a perpendicular field. Figure 3b shows the SdH oscillations as a function of $1/B$ for devices with the same doping rate (8%) as the devices used in Figure 2 and Figure 3a shows the SdH oscillations as a function of $1/B$ for devices with a lower doping rate (2%). Three resistance oscillations can be clearly observed for both devices. The amplitude of the resistance oscillations increases with N-doping, but the oscillation frequencies decrease with N-doping. We fitted the resistance oscillations with $\Delta R(B) = A \exp(-\pi/\mu B) \cos[2\pi(B_F/B) + \beta]$, where ΔR is the oscillations in resistance, B is the magnetic field, B_F is the oscillation frequency, μ is the quantum mobility, and β is the Berry phase. B_F for those two N-doped graphene devices calculated from the fitting, are 25 T (low) and 5 T (high), which correspond to 2D electron densities of 5×10^{11} and 1×10^{11} cm^{-2}, where the 2D electron density is calculated by $n = (e/h)B_F$. It is clear that N-doping decreases the 2D current density which increases the amplitude but decreases the frequency of the SdH oscillations. We also plot the SdH oscillation as a function of $1/B$ for pristine graphene in Figure 3c. One can see that the amplitude and the oscillation frequencies of pristine graphene also follow the same trend.

Angular Dependent Transport Properties at 10 K. The magneto-transport properties of the N-doped graphene were further investigated using magnetic fields rotated from out-of-plane, perpendicular to the current configuration to in-plane along the current configuration. The evolution of the MR, measured at a temperature of 10 K, as a function of the angle θ, from 0° (perpendicular field) to 90° (in-plane field), is shown in Figure 4a, where the angle θ is defined as the angle between the direction of the magnetic field and the direction normal to the graphene plane. The MR ratio decreases with increasing θ, and the WL effect is

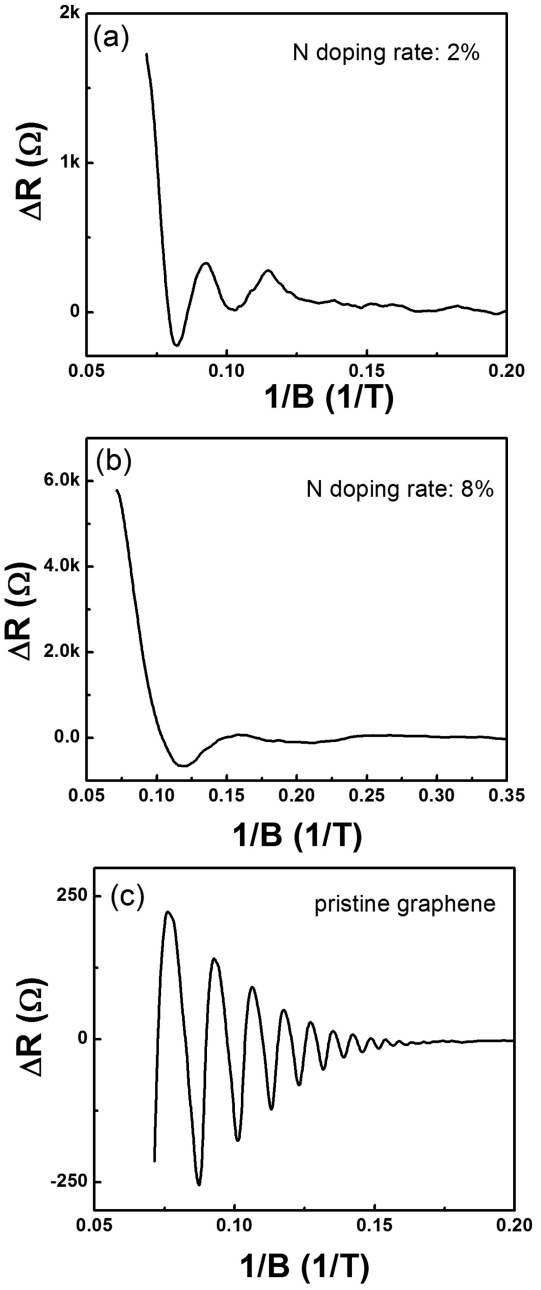

Figure 3. Effect of N-doping rate on 2D transport properties. Resistance oscillations as a function of $1/B$ at 2 K measured with the field perpendicular to the graphene plane for devices with a doping rate of 2% (a) and 8% (b). (c) Resistance oscillations as a function of $1/B$ at 2 K measured with the field perpendicular to the graphene plane for pristine graphene devices.

observed at all angles. The stepped behavior can be clearly observed when θ is less than 45°, but the field at which the step becomes apparent increases with increasing θ. For $\theta > 60°$, only quadratic MR or linear MR can be observed at high fields, given the limitation of the 14 T field available to us. Following the subtraction used in Figure 2d, we plotted the SdH oscillation as a function of $B \cos \theta$ in Figure 4b. One can see that the peaks of the SdH oscillations shift toward higher field with increasing θ, but the MR

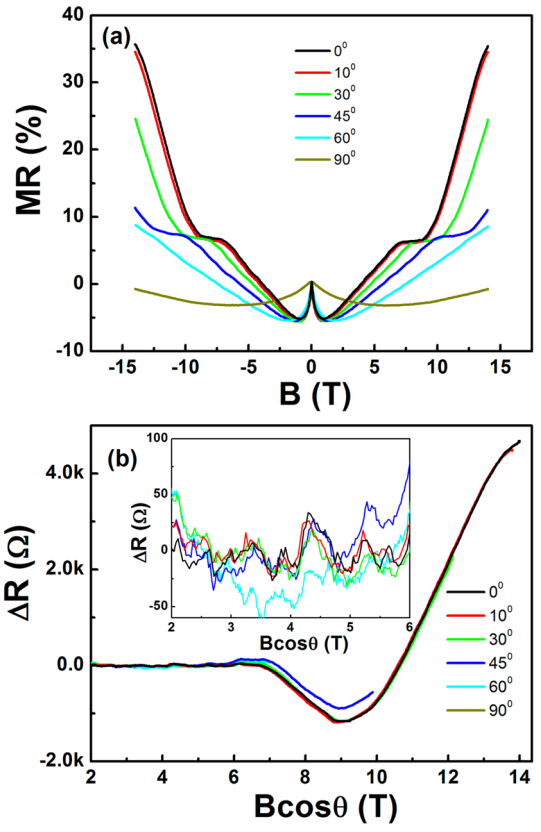

Figure 4. Angular-dependent MR of N-doped graphene at 10 K. (a) Magneto-resistance as a function of magnetic field measured with magnetic fields rotated from an out-of-plane configuration to an in-plane along the current configuration. (b) SdH oscillations at 10 K measured with magnetic fields rotated from an out-of-plane configuration to an in-plane along the current configuration. Inset: resistance oscillations at low fields.

curves remain almost exactly the same if plotted in $B\cos\theta$, even at low fields, which gives a another indication that the resistance oscillations arise from the 2D transport.

Temperature-Dependent Transport Properties. Figure 5a shows the temperature-dependent magneto-resistance as a function of magnetic field measured with a perpendicular magnetic field. Remarkably, the stepped MR behavior can be observed up to a temperature of 150 K. It has been shown by Geim *et al.* that for pristine graphene the quantum effect can be observed at room temperature under a magnetic field of 30 T or higher.[49] For our N-doped graphene, the temperature at which the quantum effect is observable is lowered due to the doping and constraint of the 14 T field available to us. To explore the underlying physics, we plotted in Figure 5b the corresponding SdH oscillations. As expected, the amplitude of the SdH oscillation decreases with increasing temperature. We summarize the thermal dependence of the amplitude of the SdH oscillation at 9 and 14 T in Figure 5c. From Figure 5c it is seen, in contrast to the well-established standard Lifshitz–Kosevich theory,[50] that the amplitude of the SdH oscillation decreases linearly with increasing temperature. We interpret this special phenomenon as follows. According to the standard Lifshitz–Kosevich theory, the amplitude of the SdH oscillation can be described as

$$\Delta R(T,B) \propto \exp[\ -2\pi^2 k_B T_D/\Delta E_N(B)]\ \frac{2\pi^2 k_B T/\Delta E_N(B)}{\sinh 2\pi^2 k_B T/\Delta E_N(B)}$$

where $\Delta E_N(B) = heB/2\pi m^*$ is the energy gap between the Nth and $(N+1)$th Landau levels, $T_D = h/4\pi^2\tau k_B$ is the Dingle temperature, m^* is the electron effective mass, h is the Planck constant, τ is the total scattering time, and k_B is the Boltzmann constant. To understand the linear temperature dependence of the amplitude of the SdH oscillation, we first assume τ is temperature dependent and focus on the factor $A_T/\sinh(A_T)$, where $A_T = 2\pi^2 k_B T/\Delta E_N(B)$. Figure S3 shows $A_T/\sinh(A_T)$ as a function of A_T. The curve shows an approximate linear relationship in the region of $A_T < 3$. It is known that the electrons within pristine graphene behave as massless Dirac Fermions. Thus, $kT \ll \hbar\omega_c$. Amplitude *versus* temperature should approach a constant. However, in our highly doped N-graphene, a bandgap may open, which results in a non-zero electron effective mass, meaning A_T becomes greater. In our experiment A_T may be smaller than 2 even at temperatures up to 150 K and under a magnetic field of 14 T, and this is coincidently the region where there is the best linearity of the curve. Second, for our highly doped N-graphene, the electronic scattering by impurities (τ) may be temperature dependent, which can lead to an increase in amplitude of the SdH oscillations with decreasing temperature. A similar effect has been found in antimony-doped bismuth single crystals.[51] In fact, for bismuth doped with 1.5% antimony, the amplitude of the SdH oscillation decreases nearly linearly with increasing temperature.

One can also note from Figure 5a that the MR ratio increases with increasing temperature. The MR ratio is around 35% at 10 K and increases to 73% at 300 K under a perpendicular magnetic field of 14 T. The increase of the MR ratio with temperature cannot be explained by the SdH oscillation as the amplitude of the SdH oscillation decreases linearly with increasing temperature. In our N-doped graphene, there are at least two distinct nitrogen configurations, *i.e.* substitutional N and weak pyridine-like N. To study the electronic structure of pyridine-like N-doped graphene, we performed the first-principle simulations. The calculations are summarized in Figure S4. Our first-principle simulations suggest that pyridine-like N can result in p-type states in graphene sheets, which is also consistent with other reports.[52] More details about the calculations can be found in the Supporting Information. Therefore, the former, substitutional N, will supply electrons, and the latter will accept electrons which will result in some localized sections of the graphene sheet

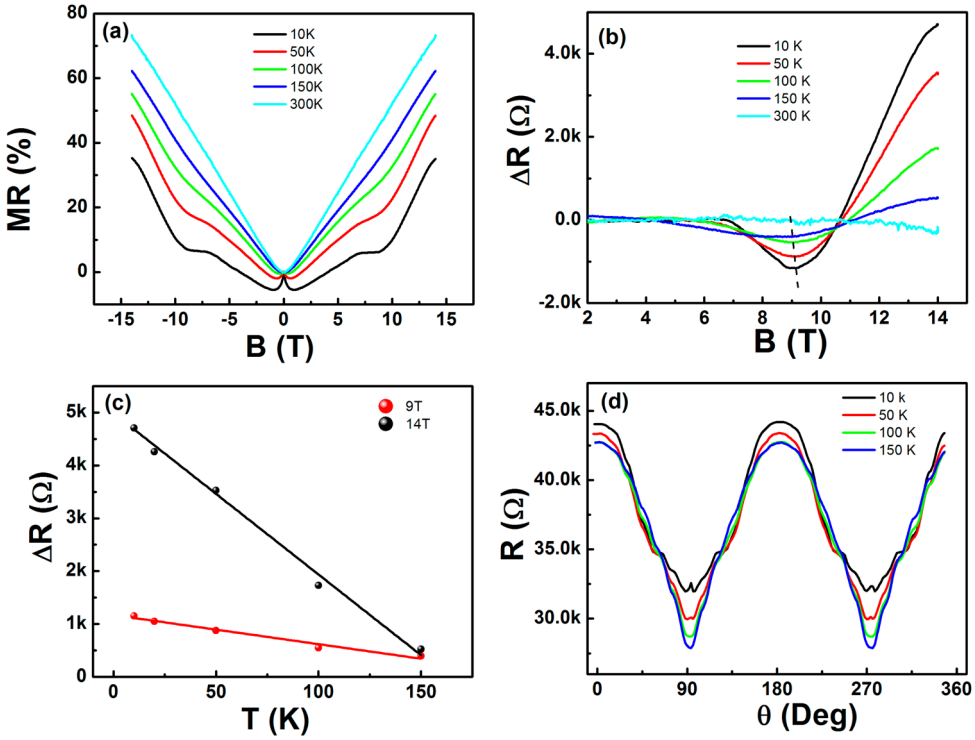

Figure 5. Temperature dependent MR of N-doped graphene. (a) Temperature-dependent magneto-resistance as a function of magnetic field measured with a perpendicular magnetic field. (b) SdH oscillations measured at a variety of temperatures with a perpendicular magnetic field. (c) SdH oscillation amplitudes at 9 and 14 T as a function of temperature. (d) Angular-dependent resistance measured at a variety of temperatures with a magnetic field of 14 T.

being in an n-type state and others adopting a p-type state. It has been suggested by Abrikosov that the field-dependent linear magneto-resistivity $\rho_i(H)$ can be written as[46]

$$\rho_i(H) = \frac{f_i(H)N_iH}{\pi(n_e - n_h)^2ec}$$

Where $f_i(H)$ are functions of the order of unity, n_e and n_h are the electron and hole densities, N_i is the density of the static scattering centers, and π, e, c have their conventional meanings. As the temperature increases, both the electrons and holes in the N-doped graphene can contribute to the transport, which decreases the difference between n_e and n_h and thus increases the MR ratio. To further explore the transport properties of N-doped graphene, Figure 5d shows the angular-dependent resistance measured at various temperatures under a magnetic field of 14 T. Compared with conventional pristine graphene, ripples and steps can be clearly observed in Figure 5d due to the enhanced SdH oscillation in the N-doped graphene. The small peaks observed at 90° are due to the weak localization effect.

CONCLUSIONS

To conclude, we experimentally investigated the magneto-transport properties of N-doped graphene. We observed an enhanced SdH oscillation. The SdH oscillation in N-doped graphene displays three interesting features. First, the amplitude of the SdH oscillation increases with N-doping and reaches around 5k Ω under a field of 14 T at 10 K. Second, in contrast to the well-established standard Lifshitz–Kosevich theory, the amplitude of SdH oscillation decreases linearly with increasing temperature. Third, the SdH oscillation persists at a temperature up to 150 K. Our results may be useful for the application of N-doped graphene in magnetic devices, such as Hall devices, magnetic sensors, *etc.*

METHODS

Graphene Transfer. The commercial N-doped graphene/Cu foil was affixed to a silicon substrate and pressed flat; this was then spin-coated with a 100 nm thick nitrocellulose polymer. After spin-coating, the Cu foil was etched using a 1 M solution of ammonium persulfate in DI water. The graphene and polymer stack was then transferred to a DI rinse for 20 min, where it was floated onto the SiO_2/Si substrate. The films were then dried in a vacuum oven for 2 h at 80 °C at a pressure of 0.1 bar. Finally, cellulose polymer films were dissolved by an 8 h immersion in acetone.

Device Fabrication. The field-effect transistor Hall bar structure was fabricated by electron beam lithography (EBL) using a single-layer negative tone resist ma-N 2403 supplied by Microchem Corp., followed by O_2 plasma etching for 60 s (8 W at P = 20 mTorr). After development, thick metal contacts consisting of Ti (5 nm)/Au (45 nm) were deposited through e-beam evaporation.

Conflict of Interest: The authors declare no competing financial interest.

Acknowledgment. We thank Prof. Alexander Grigorenko from the University of Manchester for reading this paper and giving valuable comments. This work was supported by the Beijing Institute of Technology Research Fund Program for Young Scholars and National Plan for Science and Technology (Nos. NPST 1598-02 and NPST 1466-02) of King Abdulaziz City for Science and Technology. H.C.W., M.A., and M.A. thank Saudi Aramco for financial support (Project No. 6600028398).

Supporting Information Available: Additional Raman spectra for N-doped graphene and pristine graphene, I–V curves for N-doped graphene device, and electronic structure for pyridine-like N-doped graphene are given in Figures S1–S4. The Supporting Information is available free of charge on the ACS Publications website at DOI: 10.1021/acsnano.5b02020.

REFERENCES AND NOTES

1. Novoselov, K. S.; Geim, A. K.; Morozov, S. V.; Jiang, D.; Katsnelson, M. I.; Grigorieva, I. V.; Dubonos, S. V.; Firsov, A. A. Two-Dimensional Gas of Massless Dirac Fermions in Graphene. *Nature* **2005**, *438*, 197–200.
2. Zhang, Y.; Tan, Y.-W.; Stormer, H. L.; Kim, P. Experimental Observation of the Quantum Hall Effect and Berry's Phase in Graphene. *Nature* **2005**, *438*, 201–204.
3. Stoller, M. D.; Park, S.; Zhu, Y.; An, J.; Ruoff, R. S. Graphene-Based Ultracapacitors. *Nano Lett.* **2008**, *8*, 3498.
4. Balandin, A. A.; Ghosh, S.; Bao, W.; Calizo, I.; Teweldebrhan, D.; Miao, F.; Lau, C. N. Superior Thermal Conductivity of Single-Layer Graphene. *Nano Lett.* **2008**, *8*, 902–907.
5. Bolotin, K. I.; Sikes, K. J.; Jiang, Z.; Klima, M.; Fudenberg, G.; Hone, J.; Kim, P.; Stormer, H. L. Ultrahigh Electron Mobility in Suspended Graphene. *Solid State Commun.* **2008**, *146*, 351–355.
6. Lee, C.; Wei, X.; Kysar, J. W.; Hone, J. Measurement of the Elastic Properties and Intrinsic Strength of Monolayer Graphene. *Science* **2008**, *321*, 385.
7. Kosynkin, D. V.; Higginbotham, A. L.; Sinitskii, A.; Lomeda, J. R.; Dimiev, A.; Price, B. K.; Tour, J. M. Longitudinal Unzipping of Carbon Nanotubes To Form Graphene Nanoribbons. *Nature* **2009**, *458*, 872.
8. Li, X.; Wang, X.; Zhang, L.; Lee, S.; Dai, H. Chemically Derived, Ultrasmooth Graphene Nanoribbon Semiconductors. *Science* **2008**, *319*, 1229.
9. Ponomarenko, L. A.; Schedin, F.; Katsnelson, M. I.; Yang, R.; Hill, E. W.; Novoselov, K. S.; Geim, A. K. Chaotic Dirac Billiard in Graphene Quantum Dots. *Science* **2008**, *320*, 356.
10. Ritter, K. A.; Lyding, J. W. The Influence of Edge Structure on the Electronic Properties of Graphene Quantum Dots and Nanoribbons. *Nat. Mater.* **2009**, *8*, 235.
11. Derycke, V.; Martel, R.; Appenzeller, J.; Avouris, P. Controlling Doping and Carrier Injection in Carbon Nanotube Transistors. *Appl. Phys. Lett.* **2002**, *80*, 2773.
12. Gong, K.; Du, F.; Xia, Z.; Durstock, M.; Dai, L. Nitrogen-Doped Carbon Nanotube Arrays with High Electrocatalytic Activity for Oxygen Reduction. *Science* **2009**, *323*, 760.
13. Wang, S. Y.; Wang, X.; Jiang, S. P. PtRu Nanoparticles Supported on 1-Aminopyrene- Functionalized Multiwalled Carbon Nanotubes and Their Electrocatalytic Activity for Methanol Oxidation. *Langmuir* **2008**, *24*, 10505.
14. Wang, S. Y.; Yang, F.; Chen, S. L.; Jiang, S. P.; Wang, X. Tuning the Electrocatalytic Activity of Pt Nanoparticles on Carbon Nanotubes *via* Surface Functionalization. *Electrochem. Commun.* **2010**, *12*, 1646.
15. Zhou, C.; Kong, J.; Yenilmez, E.; Dai, H. Modulated Chemical Doping of Individual Carbon Nanotubes. *Science* **2000**, *290*, 1552.
16. Panchokarla, L. S.; Subrahmanyam, K. S.; Saha, S. K.; Govindaraj, A.; Krishnamurthy, H. R.; Waghmare, U. V.; Rao, C. N. R. Synthesis, Structure, and Properties of Boron- and Nitrogen-Doped Graphene. *Adv. Mater.* **2009**, *21*, 4726–4730.
17. Wang, X. R.; Li, X. L.; Zhang, L.; Yoon, Y.; Weber, P. K.; Wang, H. L.; Guo, J.; Dai, H. J. N-Doping of Graphene Through Electrothermal Reactions with Ammonia. *Science* **2009**, *324*, 768–771.
18. Dai, J. Y.; Yuan, J. M.; Giannozzi, P. Gas Adsorption on Graphene Doped with B, N, Al, and S: A Theoretical Study. *Appl. Phys. Lett.* **2009**, *95*, 232105.
19. Zou, Y.; Li, F.; Zhu, Z. H.; Zhao, M. W.; Xu, X. G.; Su, X. Y. An *Ab Initio* Study on Gas Sensing Properties of Graphene and Si Doped Graphene. *Eur. Phys. J. B* **2011**, *81*, 475–479.
20. Meyer, J. C.; Kurasch, S.; Park, H. J.; Skakalova, V.; Kunzel, D.; Gross, A.; Chuvilin, A.; Algara-Siller, G.; Roth, S.; Iwasaki, T.; et al. Experimental Analysis of Charge Redistribution due to Chemical Bonding by High-Resolution Transmission Electron Microscopy. *Nat. Mater.* **2011**, *10*, 209–215.
21. Cui, T. X.; Lv, R. T.; Huang, Z. H.; Zhu, H. W.; Zhang, J.; Li, Z.; Jia, Y.; Kang, F. Y.; Wang, K. L.; Wu, D. H. Synthesis of Nitrogen-Doped Carbon Thin Films and Their Applications in Solar Cells. *Carbon* **2011**, *49*, 5022–5028.
22. Lv, R. T.; Cui, T. X.; Jun, M. S.; Zhang, Q.; Cao, A. Y.; Su, D. S.; Zhang, Z. J.; Yoon, S. H.; Miyawaki, J.; Mochida, I.; et al. Open-Ended, N-Doped Carbon Nanotube-Graphene Hybrid Nanostructures as High-Performance Catalyst Support. *Adv. Funct. Mater.* **2011**, *21*, 999–1006.
23. Qu, L. T.; Liu, Y.; Baek, J. B.; Dai, L. M. Nitrogen-Doped Graphene as Efficient Metal-Free Electrocatalyst for Oxygen Reduction in Fuel Cells. *ACS Nano* **2010**, *4*, 1321–1326.
24. Reddy, A. L. M.; Srivastava, A.; Gowda, S. R.; Gullapalli, H.; Dubey, M.; Ajayan, P. M. Synthesis of Nitrogen-Doped Graphene Films for Lithium Battery Application. *ACS Nano* **2010**, *4*, 6337.
25. Wu, Z. S.; Ren, W. C.; Xu, L.; Li, F.; Cheng, H. M. Doped Graphene Sheets As Anode Materials with Superhigh Rate and Large Capacity for Lithium Ion Batteries. *ACS Nano* **2011**, *5*, 5463.
26. Qie, L.; Chen, W. M.; Wang, Z. H.; Shao, Q. G.; Li, X.; Yuan, L. X.; Hu, X. L.; Zhang, W. X.; Huang, Y. H. Nitrogen-Doped Porous Carbon Nanofiber Webs as Anodes for Lithium Ion Batteries with a Superhigh Capacity and Rate Capability. *Adv. Mater.* **2012**, *24*, 2047.
27. Wang, D. W.; Gentle, I. R.; Lu, G. Q. Enhanced Electrochemical Sensitivity of PtRh Electrodes Coated with Nitrogen-Doped Graphene. *Electrochem. Commun.* **2010**, *12*, 1423.
28. Wang, Y.; Shao, Y. Y.; Matson, D. W.; Li, J. H.; Lin, Y. H. Nitrogen-Doped Graphene and Its Application in Electrochemical Biosensing. *ACS Nano* **2010**, *4*, 1790–1798.
29. Elias, A. L.; Carrero-Sanchez, J. C.; Terrones, H.; Endo, M.; Laclette, J. P.; Terrones, M. Viability Studies of Pure Carbon- and Nitrogen-Doped Nanotubes with Entamoeba Histolytica: From Amoebicidal to Biocompatible Structures. *Small* **2007**, *3*, 1723–1729.
30. Carrero-Sanchez, J. C.; Elias, A. L.; Mancilla, R.; Arrellin, G.; Terrones, H.; Laclette, J. P.; Terrones, M. Biocompatibility and Toxicological Studies of Carbon Nanotubes Doped with Nitrogen. *Nano Lett.* **2006**, *6*, 1609–1616.
31. Jeong, H. M.; Lee, J. W.; Shin, W. H.; Choi, Y. J.; Shin, H. J.; Kang, J. K.; Choi, J. W. Nitrogen-Doped Graphene for High-Performance Ultracapacitors and the Importance of Nitrogen-Doped Sites at Basal Planes. *Nano Lett.* **2011**, *11*, 2472.
32. Huang, X.; Yin, Z.; Wu, S.; Qi, X.; He, Q.; Zhang, Q.; Yan, Q.; Boey, F.; Zhang, H. Graphene-Based Materials: Synthesis, Characterization, Properties, and Applications. *Small* **2011**, *7*, 1876.
33. Guo, S.; Dong, S. Graphene Nanosheet: Synthesis, Molecular Engineering, Thin Film, Hybrids, and Energy and Analytical Applications. *Chem. Soc. Rev.* **2011**, *40*, 2644.
34. Wei, D.; Liu, Y. Controllable Synthesis of Graphene and Its Applications. *Adv. Mater.* **2010**, *22*, 3225.
35. Liu, H.; Liu, Y.; Zhu, D. Chemical Doping of Graphene. *J. Mater. Chem.* **2011**, *21*, 3335.
36. Wang, H. B.; Maiyalagan, T.; Wang, X. Review on Recent Progress in Nitrogen-Doped Graphene: Synthesis, Characterization, and Its Potential Applications. *ACS Catal.* **2012**, *2*, 781.

37. Li, X.; Zhuang, J. C.; Sun, Y.; Bai, J.; Zafar, Z. N.; Ni, Z. H.; Jin, B. B.; Shi, Z. X. Enhancement of Weak Localization for Nitrogen-Doped Graphene by Short Range Potentials. *Carbon* **2015**, *82*, 346.
38. Elias, A. L.; Ayala, P.; Zamudio, A.; Grobosch, M.; Cruz-Silva, E.; Romo-Herrera, J. M.; Campos-Delgado, J.; Terrones, H.; Pichler, T.; Terrones, M. Spectroscopic Characterization of N-Doped Single-Walled Carbon Nanotube Strands: An X-ray Photoelectron Spectroscopy and Raman Study. *J. Nanosci. Nanotechnol.* **2010**, *10*, 3959–3964.
39. Hallam, T.; Berner, N. C.; Yim, C.; Duesberg, G. S. Strain, Bubbles, Dirt, and Folds: A Study of Graphene Polymer-Assisted Transfer. *Adv. Mater. Interfaces* **2014**, *1*, 1400115.
40. Lv, R.; Li, Q.; Botello-Mendez, A. R.; Hayashi, T.; Wang, B.; Berkdemir, A.; Hao, Q. Z.; Elias, A. L.; Cruz-Silva, R.; Gutierrez, H. R.; et al. Nitrogen-Doped Graphene: Beyond Single Substitution and Enhanced Molecular Sensing. *Sci. Rep.* **2012**, *2*, 586.
41. Lucchese, M. M.; Stavale, F.; Ferreira, E. H. M.; Vilani, C.; Moutinho, M. V. O.; Capaz, R. B.; Achete, C. A.; Jorio, A. Quantifying Ion-Induced Defects and Raman Relaxation length in Graphene. *Carbon* **2010**, *48*, 1592–1597.
42. Jorio, A.; Ferreira, E. H. M.; Moutinho, M. V. O.; Stavale, F.; Achete, C. A.; Capaz, R. B. Measuring Disorder in Graphene with the G and D Bands. *Phys. Status Solidi B* **2010**, *247*, 2980–2982.
43. Dresselhaus, M. S.; Dresselhaus, G.; Hofmann, M. Raman Spectroscopy as a Probe of Graphene and Carbon Nanotubes. *Philos. Trans. A Math Phys. Eng. Sci.* **2008**, *366*, 231–236.
44. Staley, N. E.; Puls, C. P.; Liu, Y. Suppression of Conductance Fluctuation in Weakly Disordered Mesoscopic Graphene Samples Near the Charge Neutral Point. *Phys. Rev. B* **2008**, *77*, 155429.
45. Krstić, V.; Obergfell, D.; Hansel, S.; Rikken, G. L.; Blokland, J. H.; Ferreira, M. S.; Roth, S. Graphene-Metal Interface: Two-Terminal Resistance of Low-Mobility Graphene in High Magnetic Fields. *Nano Lett.* **2008**, *8*, 1700.
46. Morozov, S. V.; Novoselov, K. S.; Katsnelson, M. I.; Schedin, F.; Ponomarenko, L. A.; Jiang, D.; Geim, A. K. Strong Suppression of Weak Localization in Graphene. *Phys. Rev. Lett.* **2006**, *97*, 016801.
47. Abrikosov, A. A. Quantum Linear Magnetoresistance. *Europhys. Lett.* **2000**, *49*, 789.
48. Parish, M. M.; Littlewood, P. B. Non-Saturating Magnetoresistance in Heavily Disordered Semiconductors. *Nature* **2003**, *426*, 162.
49. Novoselov, K. S.; Jiang, Z.; Zhang, Y.; Morozov, S. V.; Stormer, H. L.; Zeitler, U.; Maan, J. C.; Boebinger, G. S.; Kim, P.; Geim, A. K. Room-Temperature Quantum Hall Effect in Graphene. *Science* **2007**, *315*, 1379.
50. Shoenberg, D. *Magnetic Oscillations in Metals*; Cambridge University Press: Cambridge, 1984.
51. Satoh, N.; Takenaka, H. Anomalous Temperature Dependence of the Amplitude of Longitudinal Shubnikov– De Haas Oscillation. *Phys. B* **2008**, *403*, 3705.
52. Fujimoto, Y.; Saito, S. Formation, Stabilities, and Electronic Properties of Nitrogen Defects in Graphene. *Phys. Rev. B* **2011**, *84*, 245446.